COMPARISON OF THEORETICAL PREDICTIONS WITH FIELD OBSERVATIONS FOR A SIMPLE FORWARD SCATTERING SENSOR

A Report to the Naval Research Laboratory
Contract # N00014-92-C-6015

by

James C. Kitchen

and

J. Ronald V. Zaneveld

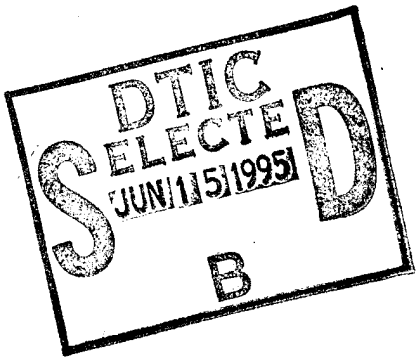

College of Oceanic and Atmospheric Sciences
Oceanography Administration Bldg 104
Oregon State University
Corvallis, Oregon 97331

Abstract

Field measurements with a simple 660 nm forward scattering sensor were analysed by means of a three-layered sphere model of light scattering. The scattering sensor measures a value that represents the scattering function multiplied by a weighting function. The geometry of the scattering sensor determines the weighting function. A model was developed that determines the weighting function based on sensor geometry. For the sensor tested the weighting function peaks at 27 degrees with a FWHM of 22 degrees.

Measurements with the device were made off the Oregon coast and off San Diego. The device tested displayed segmented linear relationships with the particulate beam attenuation coefficient at 660 nm and the particulate total scattering coefficient at 488 nm as a function of depth. The slope of the correlation with the particulate beam attenuation coefficient changed by a factor of five over a depth range of 125 meters.

The volume scattering functions off Oregon were calculated using historical data for particle size distributions and particle densities. The predicted output of the scattering sensor using the calculated scattering functions and the calculated weighting function showed that the segmented linear relationships can readily be explained by means of a change in the shape of the volume scattering function with depth.

The scattering sensor thus measures a weighted integral of the forward scattering function. Its output is dependent on both the total particle concentration and the shape of the volume scattering function in a predictable way.

Introduction

In order to rapidly assess particle fields in the ocean, a small, inexpensive, optical sensor without critical alignment problems is desired. We have data from an early prototype forward scattering sensor that satisfy these criteria. Briefly, without impinging on proprietary information, it consists of a light source, a detector and a light block in between to keep direct light from reaching the detector. This geometry is similar to the old Lamont-Daugherty nephelometers (Thorndike, 1975). This arrangement results in the reciever accepting light that depends on the geometry of the device. In the case of the instrument tested light scattered at angles between 8° and 60° is accepted with varying efficiencies. We can numerically estimate the efficiency as a function of scattering angle by dividing space up into volume elements and summing up the amount of light that would hit the detector due to scattering at each angle assuming the volume scattering function to be uniformly 1.0 m^{-1} $ster.^{-1}$. Given a real volume scattering function one could then dot multiply by the efficiency vector to obtain the signal. Effects accounted for in this program are the relative intensity of the light source in each direction, the attenuation of light from the source to the volume element and on to the detector, and the solid angle subtended by the detector as seen from the volume element.

Field test of Newport, Oregon

The first *in situ* test of this scattering sensor was carried out on August 14, 1990. Casts were made at two stations; one at 5 Nautical Miles and one at 10 NM from Newport, Oregon. In addition to scattering, we measured termperature and beam attenuation (660nm) as a function of depth. The first station (Figure 1) at 5 NM offshore was a simple three layered system with a surface turbid layer, a clearer, mid-depth layer and a bottom nepheloid layer (BNL) with the associated gradients between each. The second station (Figure 2) at 10 NM was more complex with an intermediate turbid layer between the surface turbid layer and the clean water.

Relative to the particulate attenuation, scattering is enhanced at the bottom, reduced in the intermediate turbid layer and further reduced in the surface turbid layer. The different relationships

are clearly shown in Figure 3. The linear segments in the relationship between attenuation and scattering signal are suggestive of linear mixing of water types. The region between 20 and 50 meters is suggestive of mixing of three different water types. The slopes of these relationships vary by almost a factor of five. The same plot for station 1 (Figure 4) shows just two linear relationships. The scattering signal-attenuation relationships are almost identical for the BNL's from both stations. The relationship for the inshore surface waters is similar to that for the offshore 50-90 m water. The magnitudes of these slopes are a result of the mixing process. The actual ratios (Figure 5) vary only by a factor of three.

Analysis

Without further analysis it would not be clear whether the change in the ratio of scattering signal to attenuation is due to a real change in b/c or to a change in the shape of the volume scattering function resulting in the sensor measuring a different portion of total scattering. Also, a real increase in b/c can be due to either an increase in pigment absorption per cell or a change in size distribution or more likely both.

The easiest question to answer is whether a change in the volume scattering function could acount for the observed behavior. We are very familiar with the partcle size distributions (PSD) in the coastal upwelling region (Kitchen et al., 1975, 1978; Pak et al., 1980). In surface waters PSD slopes are low in nutrient rich waters and high in relatively nutrient poor water. The high values of c and the fact that the maximum is right at the surface indicates that we are dealing with nutrient rich waters and thus low PSD slopes. The intermediate waters just below the surface layer are known to have average slopes and the BNL is known to have high slopes. We also know that the apparent density of the particles (dry weight/wet volume) increases with depth from 1.0 g/cc or less at the surface to 2.0 or more in the BNL (Peterson, 1977). From this we may infer an increase in the index of refraction of the particles. The fact that the near-surface light attenuation length is less than half a meter also suggests that the chlorophyll content of the cells should be nearly maximum.

Thus we will model the surface layer with a Junge type size distribution $dN = N_0 D^{-s} dD$ with the "slope" (s) set to 3.0. To model the diatoms which are dominant in such a system, we use a three-layered sphere (Mueller, 1974; Kitchen and Zaneveld, 1992) with a high-index of refraction outer shell, a chloroplast layer also with a relatively high index which varies according to the anomalous dispersion relations and a low-index inner core. For the intermediate waters we will use the same structure but with a slope s = 4.0. For the BNL we will use a homogeneous sphere with a uniform index of 1.09 - 0.005i and a slope s = 5.0. The resulting volume scattering functions normalized to particulate attenuation are shown in Figure 6.

The BNL has a much larger portion of its scattering in the 8-60° region, so that the scattering sensor will receive more light for the same total scattering coefficient. The mid-depth model also has significantly more scattering in this region than the near-surface model. Halving the pigment content of the near-surface model increased the portion of scattering in this range only slightly. A sensitivity function for this instrument or a very similar one (we no longer have access to design data) is shown along with a linear blowup of the volume scattering functions in Figure 7. The numerical results of meshing the sensitivity function with the volume scattering functions are given in Table I.

Table I. Predicted ratios for the various models of suspended particulates in the coastal upwelling region. BNL refers to the model for the bottom nepheloid layer; INT to the model for the intermediate layer and SUR to the surface layer. HLF is the same model as the surface layer with half the pigment concentration. SL# indicates a slope of -# for the differential particle size distribution.

	BNL SL5	INT SL4	HLF SL3	SUR SL3
scat. signal/b	0.362	0.181	0.135	0.127
scat. signal/c	0.313	0.163	0.124	0.110
b/c	0.866	0.903	0.920	0.863

The model gives almost identical results to the observations. That is, the ratio of scattering signal to total attenuation is almost three times as high in the BNL as at the surface and twice as

high at mid-depth as in the surface layer. It should be noted that the ratio of b/c varies only by a few percent even though the size distribution and pigment content were varied a great deal. We can say that changes in the particle size distribution and index of refraction are quite likely to give the results shown for the field data. That is not to say we can dismiss the other factors. Knowledge of the size distribution below 2 μm diameter is poorly known. At submicron sizes, changes in the pigment content can increase the beam attenuation with little influence on the forward scattering and thus change b/c without changing the forward portion of the volume scattering function. Also our models may not realistically proportion the chlorophyll amongst the various size classes.

Field data from off San Diego.

This scattering sensor, or a similar one, was deployed off San Diego in August 1991. Also deployed were a fluorometer, standard transmissometer (660 nm), and prototype absorption and attenuation meters (488nm) (Zaneveld et al., 1992). Station 7 was the best example of the complex structure (Figure 8) we found. There are three distinct particle maxima in the top 100 meters. Only the middle one is associated with a significant fluorescence peak. However, the scattering sensor follows the beam attenuation for both the middle and deep maxima, but is greatly reduced in the shallowest maximum. The absorption (488nm) follows the fluorescence very well (Figure 9) except thar it gives a slight indication of the third maximum while the fluorescence does not. The absorption is also slightly reduced at the surface relative to the deepest waters, while the fluorescence is slightly elevated relative to the deepest waters.

Since we have both absorption and attenuation coefficients at 488 nm we can derive the total scattering coefficient by subtraction and compare that to the measurement from the 660 nm scattering sensor (Figure 10). b(488) shows all three maxima strongly similar to c(660) while the scattering sensor measurement at 660 nm is only half as strong in the shallow maximum. Scatter plots of $c_p(488)$ and $b_p(488)$ versus $c_p(660)$ (Figure 11) show one linear relationship for the entire cast for $b_p(488)$ vs $c_p(660)$ and just a slight reduction of $c_p(488)$ vs $c_p(660)$ in the shallow maximum. The approximately 10% reduction in $b_p(488)$ can easily be attributed to changes in the

absorption spectrum. However, a plot of the scattering sensor signal (660 nm) versus the derived total scattering coefficient at 488nm (Figure 12) shows a separate linear relationship for the shallow maximum compared to the rest of the cast. The scattering sensor again showing half the signal in the shallow maximum as in the rest of the cast. Since the absorption and fluorescence is low here it would be hard to attribute this to anomalous dispersion or refraction effects. Thus, the data from this cruise gives even stronger evidence that the anomalies in the scattering sensor are due to changes in the volume scattering function and are not reflections of the behavior of particle concentration or total scattering coefficients.

It would have been interesting to simultaneously deploy scattering sensors weighted more towards smaller angles, which was in fact attempted. However, the newer sensors failed each time and thus we are left with only data from the older design.

Conclusions

1) The relationship of the output of the scattering sensor can be modeled by means of an analysis of its geometry and a knowledge of the nature of the particles being measured.

2) A scattering sensor measuring at the middle forward angles cannot be expected to yield more than a qualitative picture of the particle concentration or total scattering coefficient profiles due to variations in the shape of the volume scattering function.

3) Scattering sensors may provide extremely interesting information if the appropriate ancillary measurements are taken to make an interpretation of the signal possible.

REFERENCES

Kitchen, J.C., D. Menzies, H. Pak and J.R.V. Zaneveld (1975) Particle size distributions in a region of coastal upwelling analyzed by characteristic vectors. *Limnol. Oceanogr.*, **20**, 775-783.

Kitchen, J. C. and J. R. V. Zaneveld (1992) A Three-Layered Sphere Model of the Optical Properties of Phytoplankton. *Limnol. Oceanogr.*, **37**, 1680-1690.

Kitchen, J.C., J.R.V. Zaneveld and H. Pak (1978) The vertical structure and size distributions of suspended particles off Oregon during the upwelling season. *Deep-Sea Res.*, **25**, 453-468.

Mueller, J. L. (1974) The influence of phytoplankton on ocean color spectra. Ph.D. Thesis, Oregon State Univ. Corvallis, OR, 239 pp.

Pak, H., J.R.V. Zaneveld and J. Kitchen (1980) Intermediate nepheloid layers observed off Oregon and Washington. *J. Geophys. Res.*, **85**(C11), 6697-6708.

Peterson, R. E. (1977) A study of suspended particulate matter: Arctic Ocean and Northern Oregon Continental Shelf. Ph.D. Thesis, Oregon State University, Corvallis, OR, 122 pp..

Thorndike, E.M. (1975) A deep sea photographic nephelometer. Ocean Eng.,**3**, 1-15.

Zaneveld, J. R. V., J. C. Kitchen, A. Bricaud and C. Moore (1992) Analysis of *in situ* spectral absorption meter data. *Ocean Optics XI*, G. D. Gilbert, Ed., Proc. SPIE **1750**, 187-200.

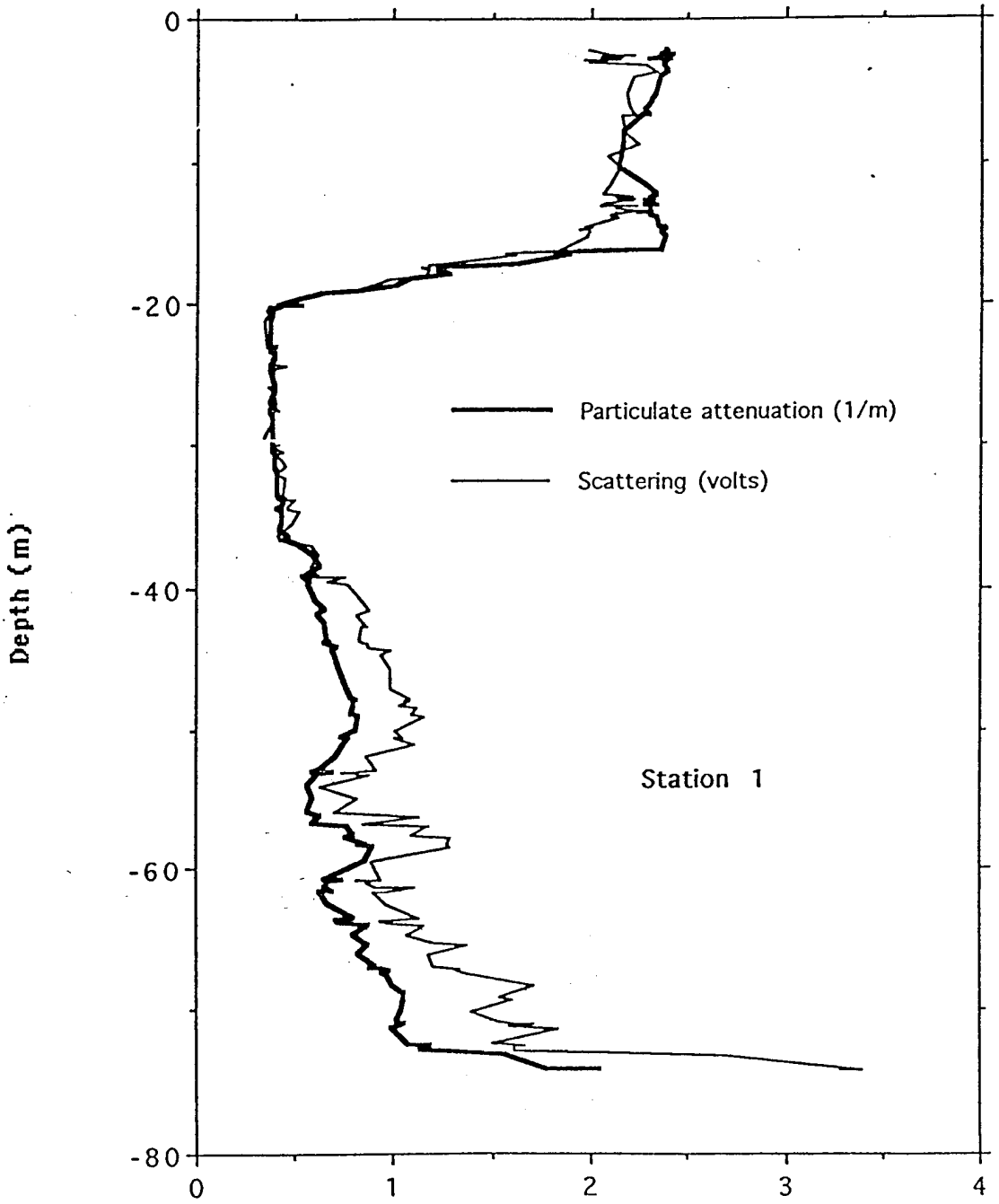

Figure 1. Profiles of the beam attenuation coefficient at 660 nm (m^{-1}) and the output of the scattering sensor (V) as a function of depth taken on August 14, 1990 5 NM off Newport, Oregon.

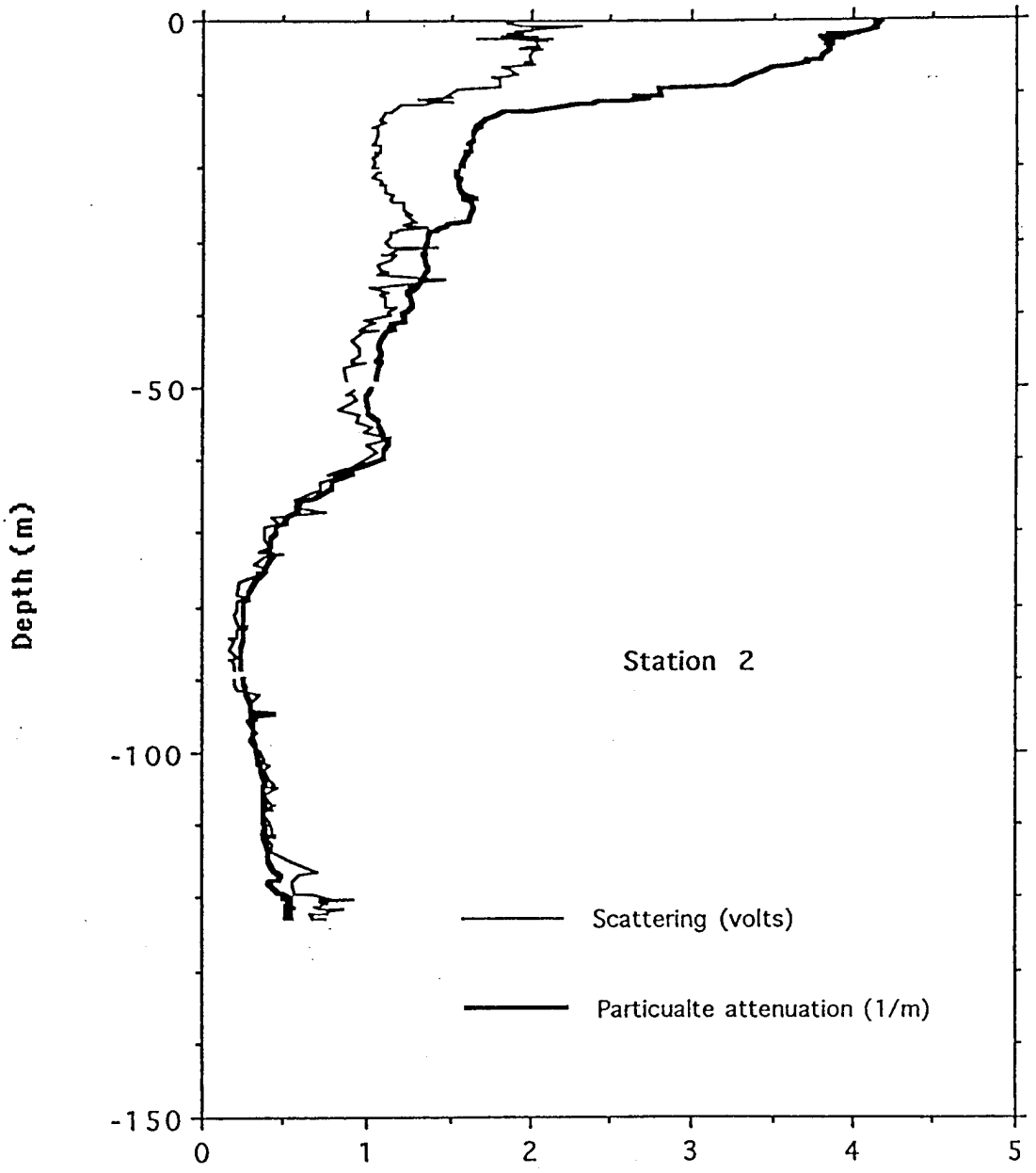

Figure 2. Profiles of the beam attenuation coefficient at 660 nm (m^{-1}) and the output of the scattering sensor (V) as a function of depth taken on August 14, 1990 10 NM off Newport, Oregon.

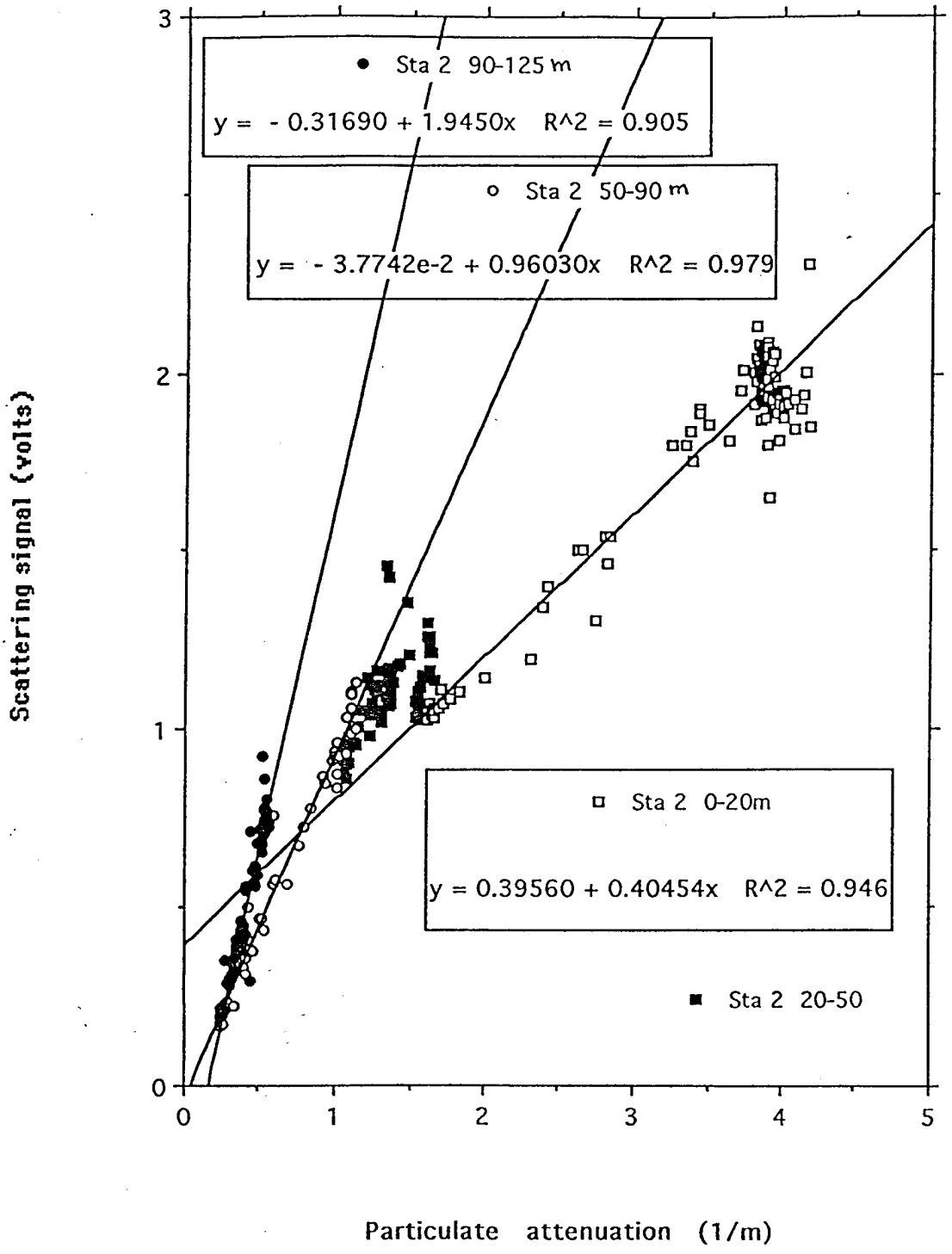

Figure 3. Scatter plots and regressions for various depth intervals of the particulate beam attenuation coefficient at 660 nm (m^{-1}) and the output of the scattering sensor (V) taken on August 14, 1990 10 NM off Newport, Oregon.

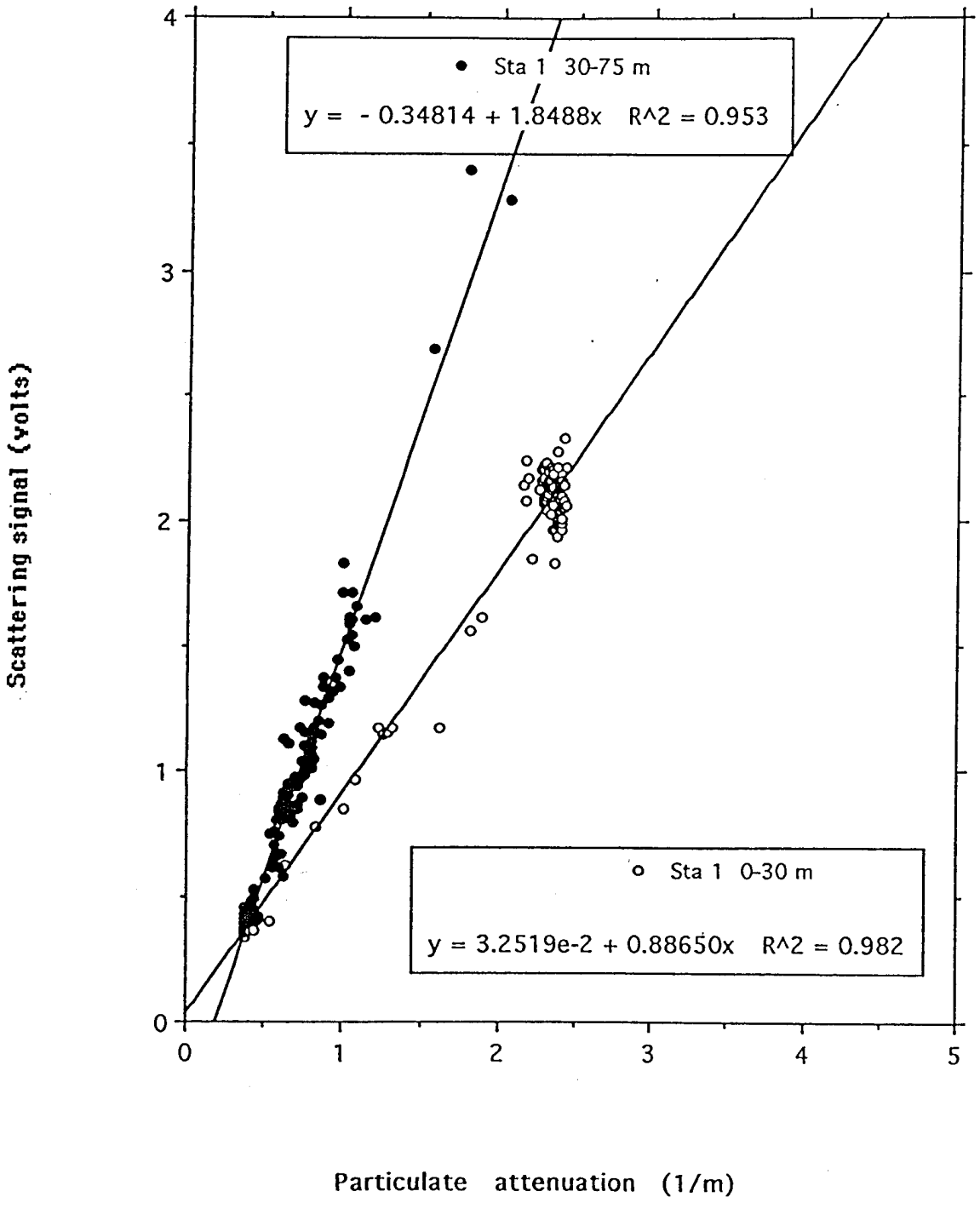

Figure 4. Scatter plots and regressions for various depth intervals of the particulate beam attenuation coefficient at 660 nm (m^{-1}) and the output of the scattering sensor (V) taken on August 14, 1990 5 NM off Newport, Oregon.

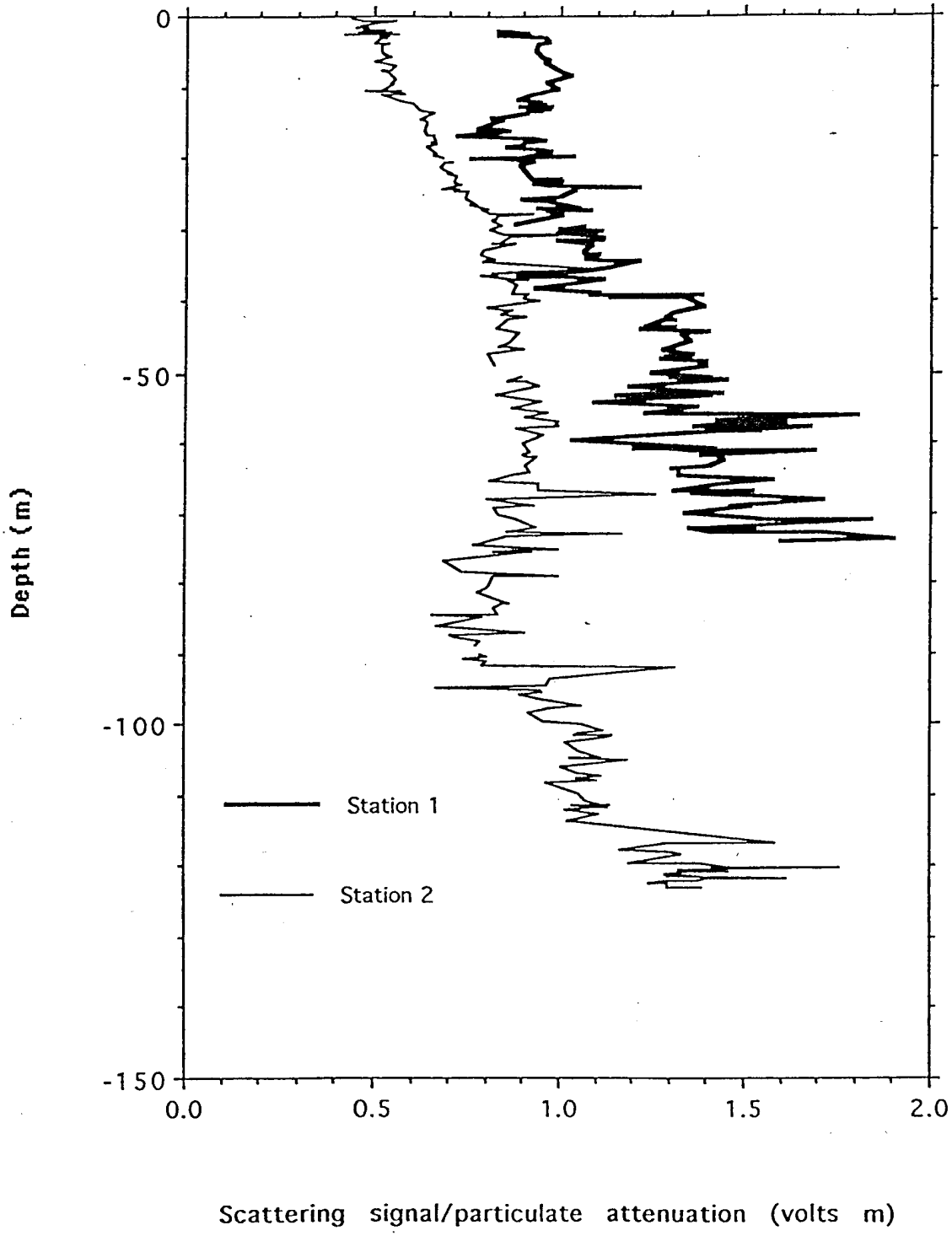

Figure 5. Ratios of the output of the scattering sensor (V) and the particulate beam attenuation coefficient at 660 nm (m^{-1}) for the two stations shown in figures 1 and 2.

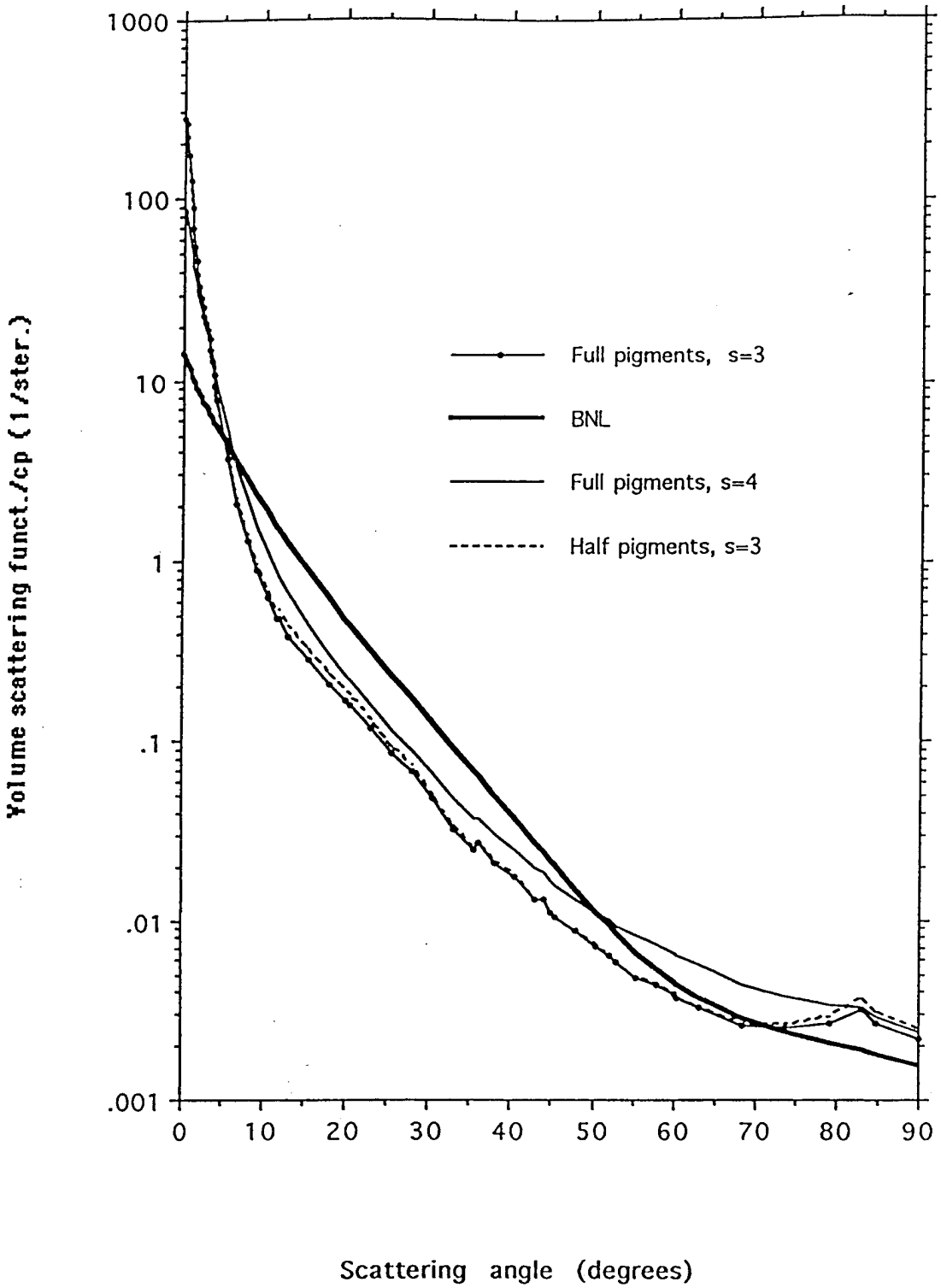

Figure 6. Volume scattering functions calculated with a three layered sphere model for the Bottom Nepheloid Layer (BNL), the intermediate water (Full pigments s=3), the surface water (Full pigments s=4) and the surface water with half of the pigments (Half pigments, s=3). For details see text.

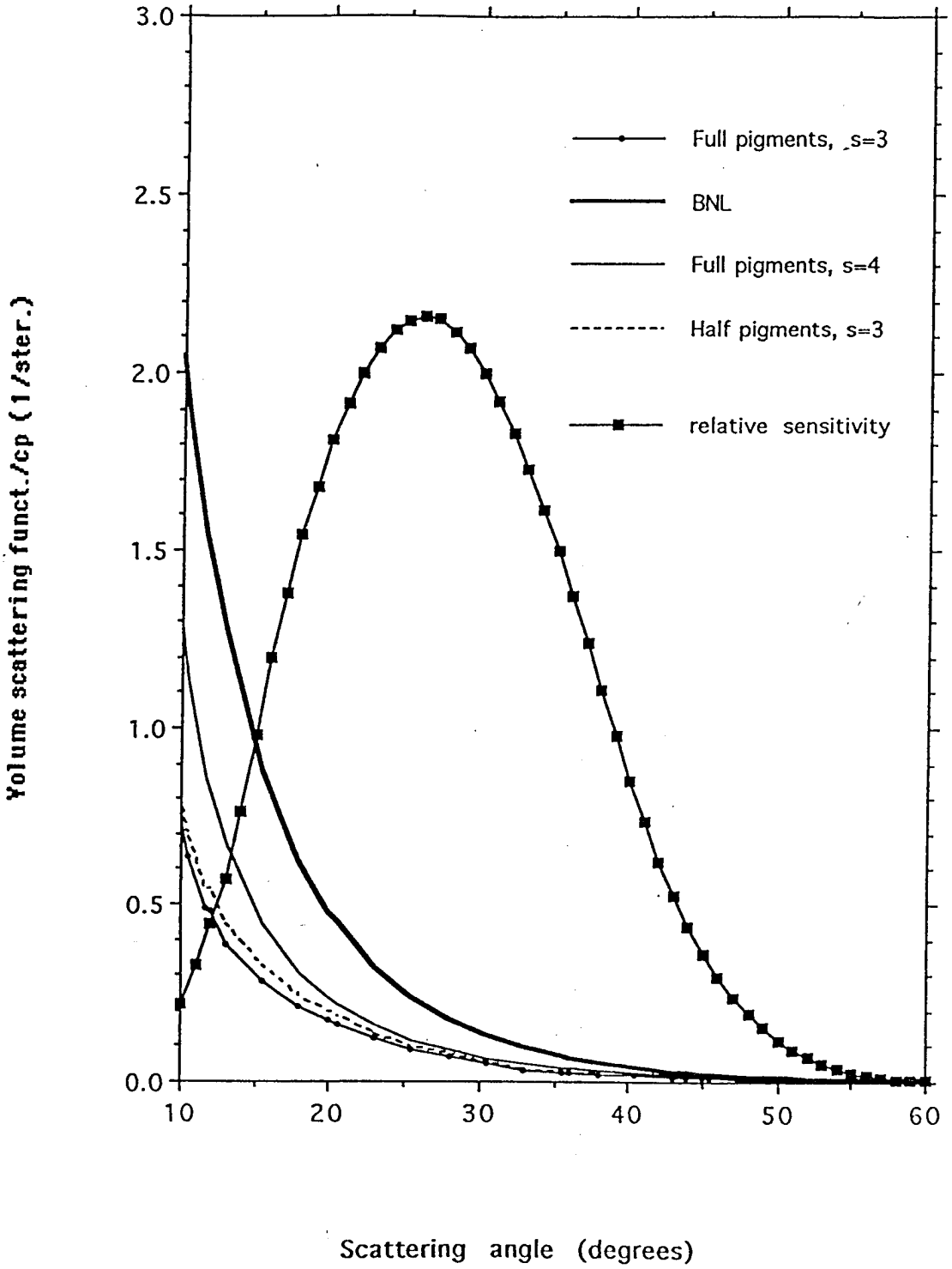

Figure 7. The calculated relative sensitivity of the scattering sensor and the volume scattering functions shown on figure 6.

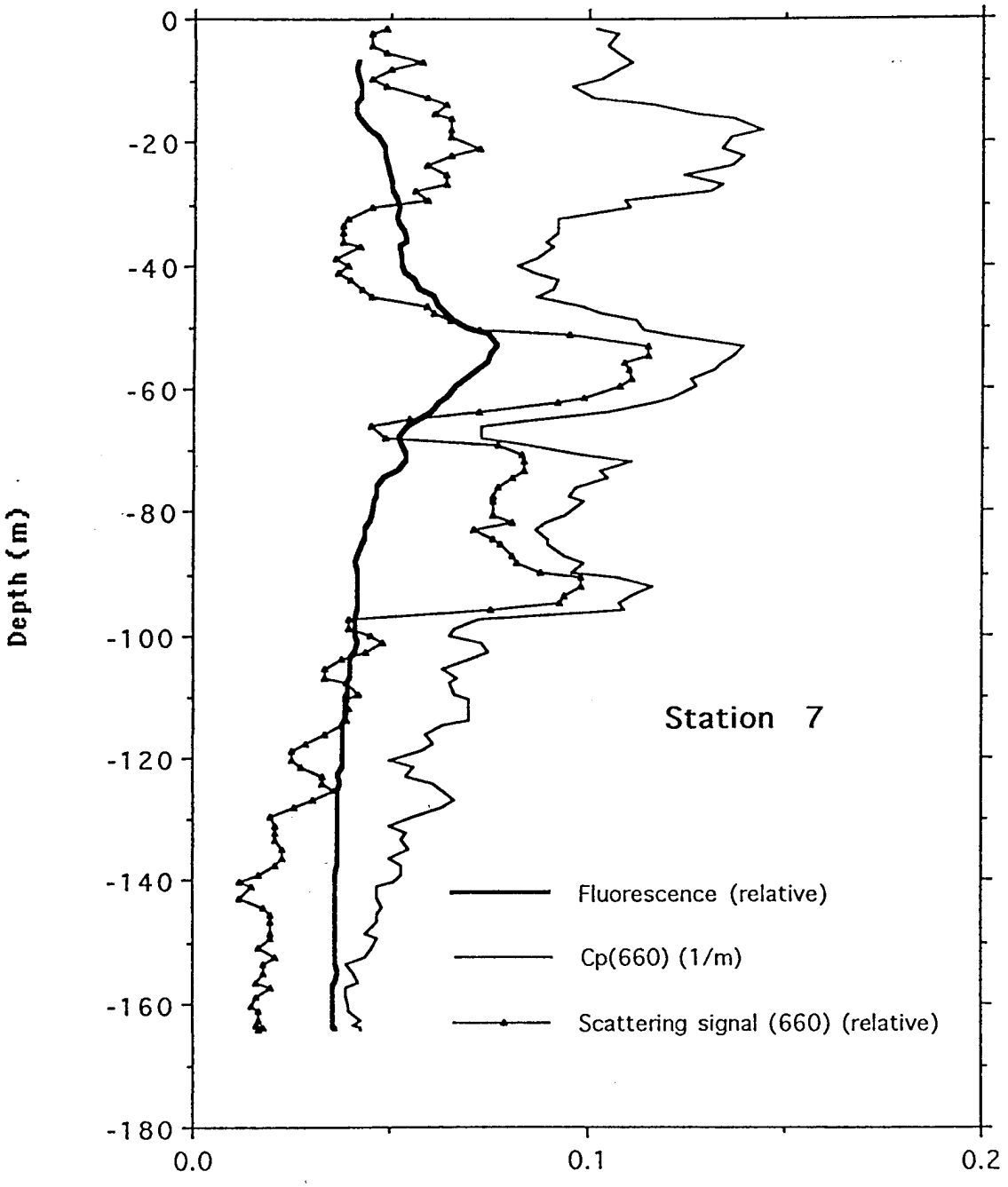

Figure 8. Profiles of stimulated fluorescence (relative units), the particulate beam attenuation coefficient at 660 nm (m^{-1}) and the output of the scattering sensor (V) as a function of depth taken during August , 1990 20 NM Southwest of San Diego, Cal.

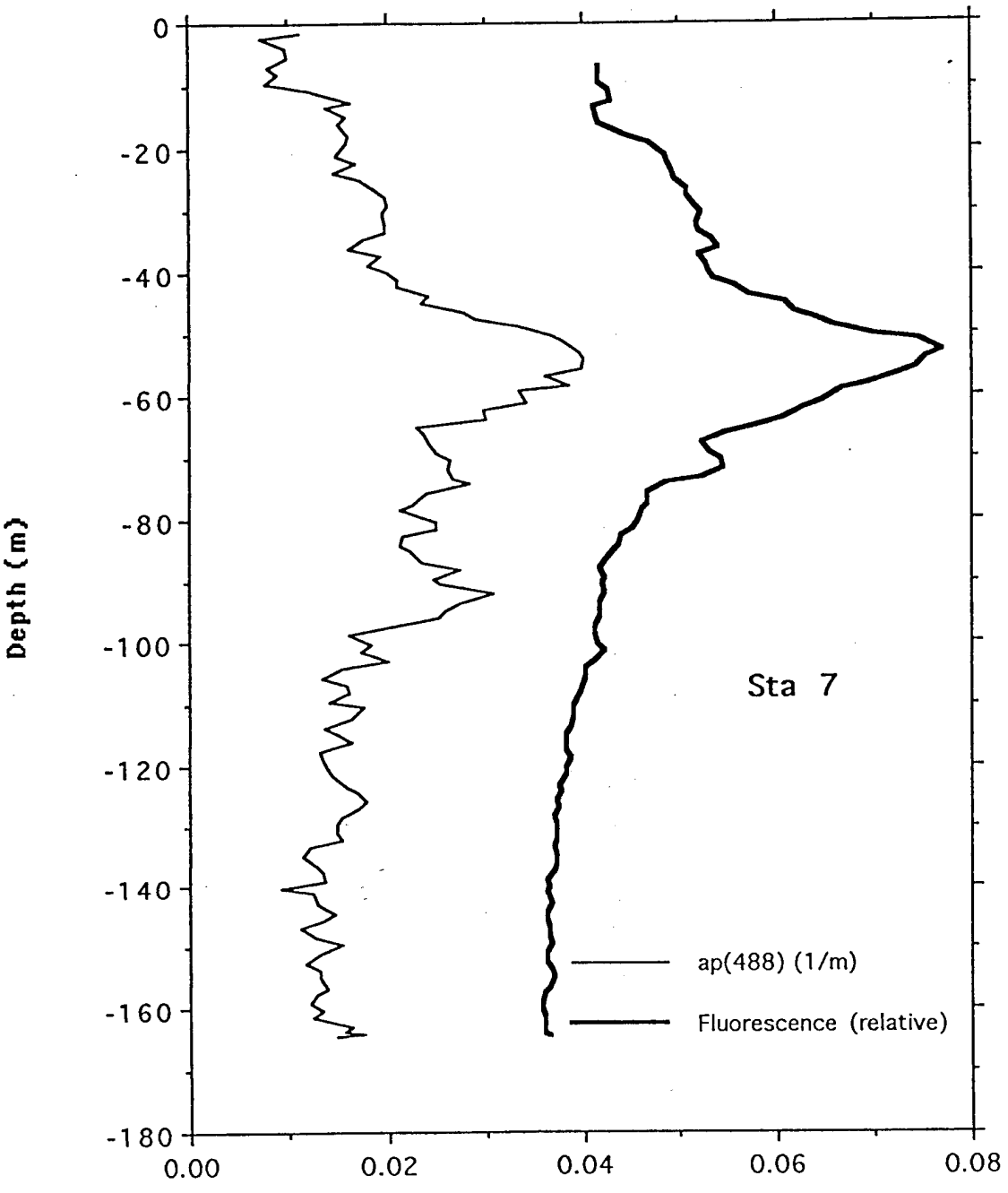

Figure 9. Profiles of stimulated fluorescence (relative units), and the particulate absorption coefficient at 488 nm (m^{-1}) as a function of depth taken during August , 1990 20 NM Southwest of San Diego, Cal.

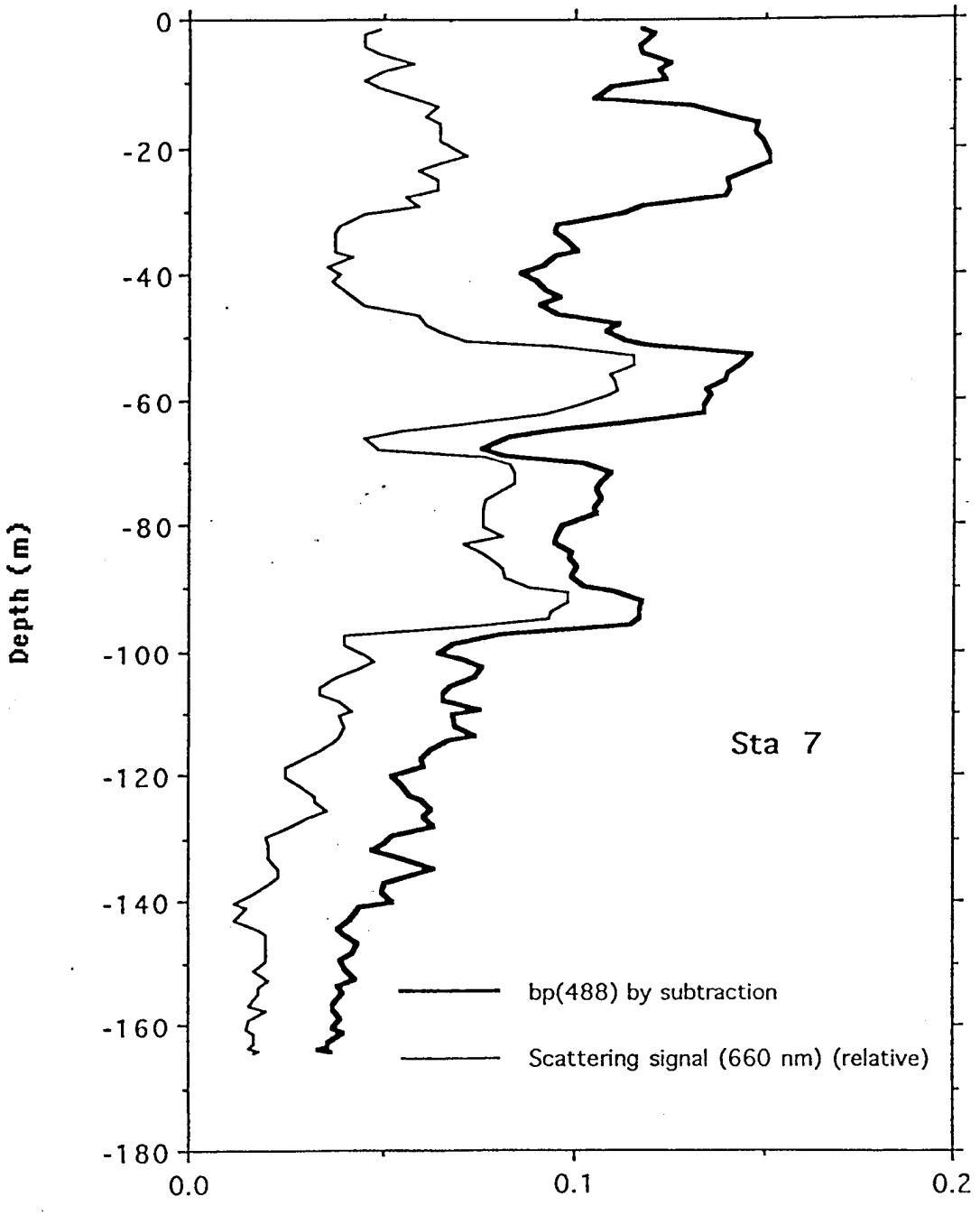

Figure 10. Profiles of the particulate total scattering coefficient at 488 nm (m^{-1}) and the output of the scattering sensor (V) as a function of depth taken during August , 1990 20 NM Southwest of San Diego, Cal.

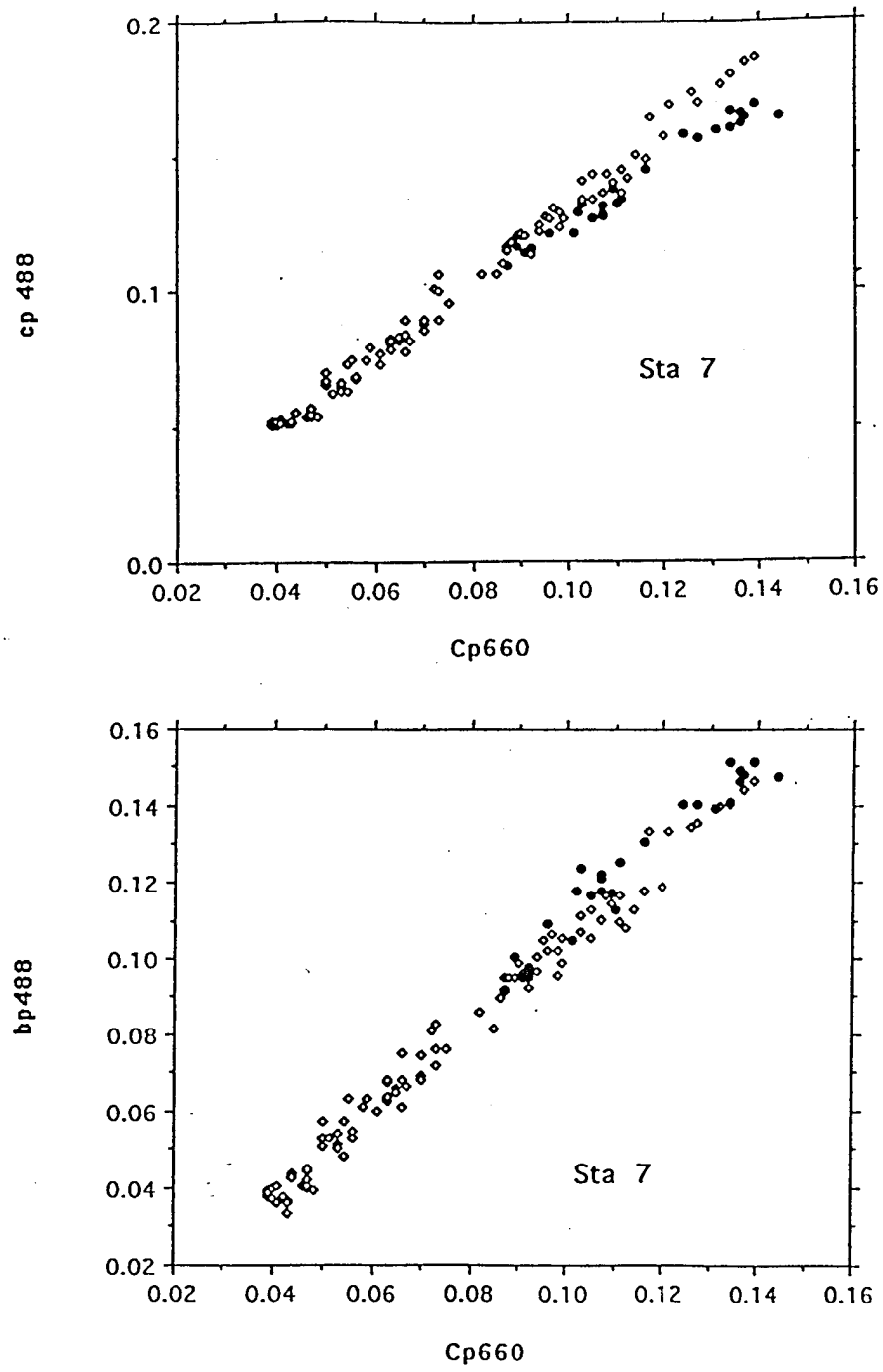

Figure 11. Upper panel. Scatter plot of the particulate beam attenuation coefficient at 488 nm as a function of the particulate beam attenuation coefficient at 660 nm for data taken during August, 1990 20 NM Southwest of San Diego, Cal. Lower panel. Scatter plot of the particulate total scattering coefficient at 488 nm as a function of the particulate beam attenuation coefficient at 660 nm for data taken during August , 1990 20 NM Southwest of San Diego, Cal.

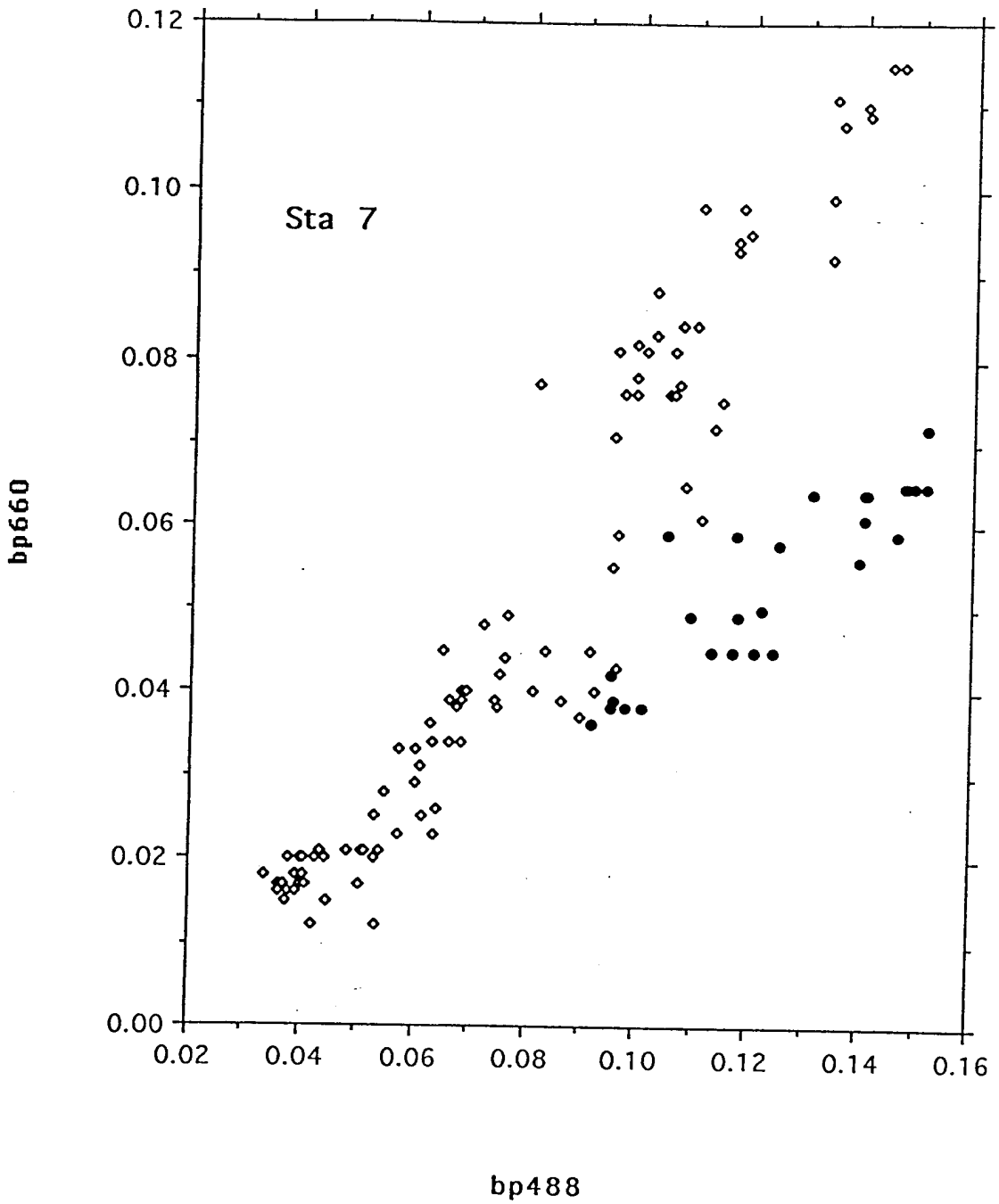

Figure 12. Scatter plot of the output of the scattering sensor at 660 nm as a function of the particulate total scattering coefficient at 488 nm for data taken during August, 1990 20 NM Southwest of San Diego, Cal.

REPORT DOCUMENTATION PAGE

Form Approved
OBM No. 0704-0188

1. AGENCY USE ONLY *(Leave blank)*	2. REPORT DATE	3. REPORT TYPE AND DATES COVERED
	Nov. 4, 1994	Contractor Report

4. TITLE AND SUBTITLE

Comparison of Theoretical Predictions with Field Observations for a Simple Forward Scattering Sensor

5. FUNDING NUMBERS

Job Order No. 74513804
Program Element No. 0604218N
Project No.
Task No. R17400S
Accession No. DN153-136

6. AUTHOR(S)

James C. Kitchen and J. Ronald Zaneveld

7. PERFORMING ORGANIZATION NAME(S) AND ADDRESS(ES)

College of Oceanic and Atmospheric Sciences
Oceanography Admin. Bldg. Oregon State University
Corvallis, Oregon 97331

8. PERFORMING ORGANIZATION REPORT NUMBER

NRL/CR/7410--94-0028

9. SPONSORING/MONITORING AGENCY NAME(S) AND ADDRESS(ES)

Office of the Chief of Naval Research
800 N. Quincy Street
Arlington, VA 22217

10. SPONSORING/MONITORING AGENCY REPORT NUMBER

11. SUPPLEMENTARY NOTES

A Report to the Naval Research Laboratory
Contract #N00014-92-C-6015

12a. DISTRIBUTION/AVAILABILITY STATEMENT

Approved for public release; distribution unlimited.

12b. DISTRIBUTION CODE

13. ABSTRACT *(Maximum 200 words)*

Field measurements with a simple 660 nm forward scattering sensor were analyzed by means of a three-layered sphere model of light scattering. The scattering sensor measures a value that represents the scattering function multiplied by a weighting function. The geometry of the scattering sensor determines the weighting function. A model was developed that determines the weighting function based on sensor geometry. For the sensor tested the weighting function peaks at 27 degrees with a FWHM of 22 degrees.

Measurements with the device were made off the Oregon coast and off San Diego. The device tested displayed segmented linear relationships with the particulate beam attenuation coefficient at 660 nm and the particulate total scattering coefficient at 488 nm as a function of depth. The slope of the correlation with the particulate beam attenuation coefficient changed by a factor of five over a depth range of 125 meters.

The volume scattering functions off Oregon were calculated using historical data for particle size distributions and particle densities. The predicted output of the scattering sensor using the calculated scattering functions and the calculated weighting function showed that the segmented linear relationships can readily be explained by means of a change in the shape of the volume scattering function with depth.

The scattering sensor thus measures a weighted integral of the forward scattering function. Its output is dependent on both the total particle concentration and the shape of the volume scattering function in a predictable way.

14. SUBJECT TERMS

tactical oceanography; dynamical oceanography; physical oceanography; electronic/electrical engineering

15. NUMBER OF PAGES

20

16. PRICE CODE

17. SECURITY CLASSIFICATION OF REPORT	18. SECURITY CLASSIFICATION OF THIS PAGE	19. SECURITY CLASSIFICATION OF ABSTRACT	20. LIMITATION OF ABSTRACT
Unclassified	Unclassified	Unclassified	SAR